

Chiral Supersolid in Spin-Orbit-Coupled Soft-Core Bose Gases

Wei Han,^{1,2} Xiao-Fei Zhang,^{1,2,*} Deng-Shan Wang,³ Hai-Feng Jiang,^{1,2} Wei Zhang,^{4,†} and Shou-Gang Zhang^{1,2,‡}

¹Key Laboratory of Time and Frequency Primary Standards,
National Time Service Center, Chinese Academy of Sciences, Xi'an 710600, China

²University of Chinese Academy of Sciences, Beijing 100049, China

³School of Science, Beijing Information Science and Technology University, Beijing 100192, China

⁴Department of Physics, Renmin University of China, Beijing 100872, China

Chirality represents a kind of symmetry breaking characterized by the non-coincidence of an object with its mirror image, and has been attracting intense attention in a broad range of scientific areas. The recent realization of spin-orbit coupling in ultracold atomic gases provides a new perspective to study quantum states with chirality. In this Letter, we demonstrate that the combined effects of spin-orbit coupling and interatomic soft-core interaction can induce an exotic supersolid phase, in which the chiral symmetry is broken and accompanied by the spontaneous emergence of circulating particle current. This implies that a finite angular momentum is generated in a non-rotating frame. More surprisingly, it is found that the direction of the angular momentum can be altered by adjusting the strengths of spin-orbit coupling or interatomic interaction. The predicted chiral supersolid phase can be experimentally observed in Rydberg-dressed Bose-Einstein condensates with spin-orbit coupling.

PACS numbers: 03.75.Lm, 67.85.Fg, 67.80.K-, 03.75.Nt

Introduction.—Chirality is a universal and fascinating phenomenon in nature [1, 2]. Exploring and investigating new states of matter with chirality is a forward subject in physics, and can light the way to a deeper understanding of nature and provide clues for designing novel functional materials. The recent discovery of exotic chiral matters, involving chiral superconductor [3], chiral electron [4], chiral domain wall [5–7] and chiral skyrmion [8], has attracted extensive interests of physicists. In many of these systems, the existence of spin-orbit (SO) coupling plays an important role in the symmetry breaking of chirality. Recent experimental realization of SO coupling in ultracold quantum gases [9–13] provides a highly controllable platform for the study of chirality [14, 15].

Even though there are plenty of studies on SO coupling, most existing works focus only on hard-core systems, where the interatomic interaction is manifested as zero-range contact [16–23] or long-range dipolar potentials [24–26]. However, soft-core interaction can also be realized in Bose gases with Rydberg dressing technology [27–30]. The essential difference between the hard-core and soft-core interactions is the behavior of potential when two atoms are brought to close distance. For the hard-core case, the interaction tends to infinity, while for soft-core systems, the interaction potential tends to a finite value. Previous investigations suggested that the soft-core interaction can induce spontaneous supersolid, which is a long-sought exotic phase of matter that behaves simultaneously as a solid and a friction-free superfluid [29–35]. With the new ingredient of SO coupling, an intriguing question is can we have a supersolid phase with chiral symmetry breaking in a soft-core Bose gas?

In this Letter, we investigate the ground-state quantum phases of soft-core Bose gases with SO coupling. A surprising finding is that the combined effects of SO

coupling and soft-core interaction can lead to a chiral supersolid (CSS), in which spontaneous circulation with broken chiral symmetry emerges in each crystal cell. This implies that a finite angular momentum is generated in a non-rotating frame, which is in stark contrast to the general expectation that the ground state of a many-body system cannot possess finite total angular momentum [36, 37], and also goes beyond the traditional means of yielding angular momentum by external rotation [38, 39] or synthetic magnetic fields [40]. More surprisingly, the direction of the angular momentum is associated with the form of phase separation, and can be altered by adjusting the strengths of SO coupling or interatomic interaction. In addition, it is revealed that the Rashba and Dresselhaus SO couplings lead to opposite chiralities of the particle currents.

Model.—We consider a homogeneous two-dimensional (2D) SO-coupled Bose-Einstein condensate (BEC) with soft-core interactions [41]. The Hamiltonian reads in the Gross-Pitaevskii mean-field approximation as

$$\begin{aligned} \mathcal{H} = & \int d\mathbf{r} \Psi^\dagger \left(-\frac{\hbar^2 \nabla^2}{2M} + \mathcal{V}_{\text{so}} \right) \Psi \\ & + \frac{1}{2} \int d\mathbf{r} \sum_{i,j=\uparrow,\downarrow} g_{ij} \Psi_i^*(\mathbf{r}) \Psi_j^*(\mathbf{r}) \Psi_j(\mathbf{r}) \Psi_i(\mathbf{r}) \\ & + \frac{1}{2} \int d\mathbf{r} d\mathbf{r}' \sum_{i,j=\uparrow,\downarrow} \Psi_i^*(\mathbf{r}) \Psi_j^*(\mathbf{r}') U_{ij}(\mathbf{r}-\mathbf{r}') \Psi_j(\mathbf{r}') \Psi_i(\mathbf{r}), \end{aligned} \quad (1)$$

where $\Psi = [\Psi_\uparrow(\mathbf{r}), \Psi_\downarrow(\mathbf{r})]^\top$ with $\mathbf{r} = (x, y)$ denotes the spinor order parameter, and is normalized to satisfy $\int d\mathbf{r} \Psi^\dagger \Psi = N$. The SO coupling term can be written as $\mathcal{V}_{\text{so}} = -i\hbar\kappa(\sigma_x \partial_x \pm \sigma_y \partial_y)$, where $\sigma_{x,y}$ are the Pauli matrices and κ denotes the SO coupling strength. Here the sign “ \pm ” distinguishes the types of SO coupling as Rashba for “ $+$ ” and Dresselhaus for “ $-$ ”. The strength of the con-

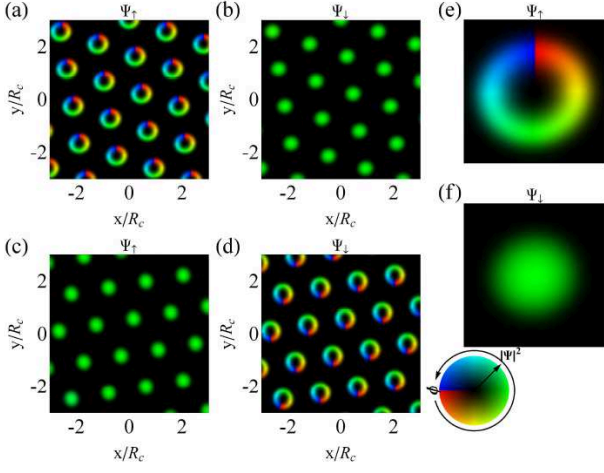


FIG. 1: (Color online) Chiral supersolid induced by Rashba spin-orbit coupling and soft-core interactions. (a)-(d) The density and phase distributions with the intra-component soft-core interactions $\tilde{C}_6^{(\uparrow\uparrow)}N = 2500 \hbar^2 R_c^4/M$, $\tilde{C}_6^{(\downarrow\downarrow)}N = 1250 \hbar^2 R_c^4/M$ in (a) and (b), and $\tilde{C}_6^{(\uparrow\uparrow)}N = 1250 \hbar^2 R_c^4/M$, $\tilde{C}_6^{(\downarrow\downarrow)}N = 2500 \hbar^2 R_c^4/M$ in (c) and (d). (e)-(f) One crystal cell of the chiral supersolid described in (a) and (b). The density and phase are represented by brightness and color, respectively. The arrows in the colour wheel point in the direction of values increasing. Other parameters are fixed at $\tilde{C}_6^{(\uparrow\downarrow)}N = 1250 \hbar^2 R_c^4/M$, $\kappa = 4 \hbar/MR_c$ and $gN = 1000 \hbar^2/M$.

tact interaction is characterized by g_{ij} , and here we focus on the SU(2) symmetric case with $g = g_{\uparrow\uparrow} = g_{\downarrow\downarrow} = g_{\uparrow\downarrow}$. The effective potential describing the soft-core interaction is written as $U_{ij}(\mathbf{r}) = \tilde{C}_6^{(ij)} / (R_c^6 + |\mathbf{r}|^6)$, where $\tilde{C}_6^{(ij)}$ characterizes the interaction strength and R_c represents the blockade radius [28].

Chiral supersolid.—By numerically minimizing the Hamiltonian functional given by Eq. (1), one can obtain the many-body ground states [41]. A primary finding is the existence of an exotic supersolid phase with chiral symmetry breaking as shown in Fig. 1. In this phase, the two spin components are separated along the radial direction in each crystal cell, with one component surrounding the other to form a ring structure. This form of phase separation is attributed to the choice of unequal intra-component soft-core interactions, and the component with weaker intra-component interaction is always surrounded by the stronger one [See Figs. 1(a)-1(d)]. While the phase of the spherical component is trivial, there exists a 2π phase gradient along a closed path around the spin-polarized core in the toroidal component, forming a vortex in each crystal cell [See Figs. 1(e)-1(f)]. Each crystal cell of the supersolid is very similar to the half-quantum vortex predicted in SO-coupled condensates with a strong harmonic trap [53–56]. It is noted that the circulating direction of the superfluid velocity in the vortex is related to the spin orientation in the vortex core, and they satisfy the right-hand rule [57].

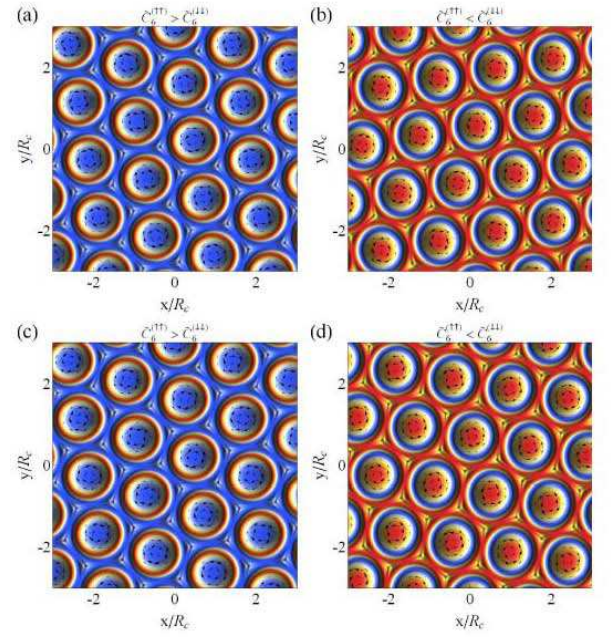


FIG. 2: (Color online) Particle currents \mathbf{j} and longitudinal magnetizations S_z of the spin induced by (a) and (b) Rashba SO coupling, (c) and (d) Dresselhaus SO coupling. The colour map and black arrows represent S_z and \mathbf{j} respectively, where the colors ranging from blue to red describe the values from -1 to 1. Parameters used are identical to those in Fig. 1. As the SO coupling is strong, the gauge part \mathbf{j}_s plays a dominated role in contributing to the total particle current \mathbf{j} . The circulating direction of the particle current and the spin orientation in the vortex core satisfy the left-hand rule in (a) and (b), the right-hand rule in (c) and (d).

A surprising observation is that the forms of phase separation for all crystal cells are coincident, thus all vortices in the supersolid crystal have the same direction and provide finite net angular momentum in the system with the chiral symmetry broken. This is distinct from the vortex lattices in an SO-coupled hard-core system, where vortices and antivortices emergence in pairs, thus provide zero net angular momentum [54, 55, 58–63]. The creation of vortex lattices with finite angular momentum is attributed to the combined effects of the SO coupling and interatomic soft-core interactions. This goes beyond the conventional view that an external rotation [38, 39] or an effective gauge magnetic field [40] is necessary to create a vortex lattice with all vortices rotating in the same direction.

According to the hydrodynamic theory [14, 64, 65], the actual particle current in an SO-coupled system is given by $\mathbf{j} = \mathbf{j}_v + \mathbf{j}_s = \rho(\mathbf{v} + \kappa\mathbf{S})$ with $\rho = |\Psi|^2$, \mathbf{v} representing the superfluid velocity and $\mathbf{S} = \Psi^\dagger \boldsymbol{\sigma} \Psi / |\Psi|^2$ being the normalized spin density vectors. Apparently, while the superfluid velocity contribution \mathbf{j}_v is maintained, the gauge term \mathbf{j}_s is in direct proportion to the SO coupling strength, and will play a dominated role for larger κ . It

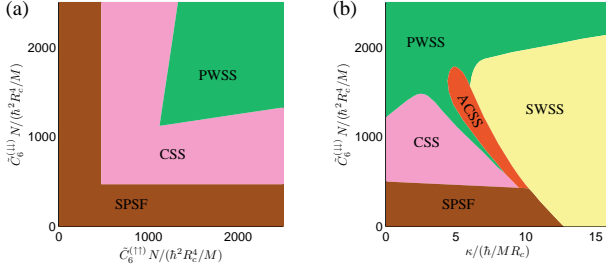


FIG. 3: (Color online) (a) Phase diagram by varying the intra-component soft-core interaction strengths $\tilde{C}_6^{(\uparrow\uparrow)}$ and $\tilde{C}_6^{(\downarrow\downarrow)}$. (b) Phase diagram by varying the Rashba SO coupling strength κ and the spin-down-component soft-core interaction strength $\tilde{C}_6^{(\downarrow\downarrow)}$. The SO coupling strength is fixed at $\kappa = 4 \hbar / M R_c$ in (a), and the spin-up-component soft-core interaction strength is fixed at $\tilde{C}_6^{(\uparrow\uparrow)} N = 2500 \hbar^2 R_c^4 / M$ in (b). Other parameters are taken as $\tilde{C}_6^{(\uparrow\downarrow)} N = 1250 \hbar^2 R_c^4 / M$ and $gN = 1000 \hbar^2 / M$.

is found that the circulating direction of the gauge part \mathbf{j}_s and the spin orientation in the vortex core satisfy the left-hand rule [See Figs. 2(a)-2(b)]. The opposite chirality between the superfluid velocity and gauge contributions to the particle current can be understood by noting that the opposite directions of \mathbf{j}_v and \mathbf{j}_s will lead to a minimal particle current \mathbf{j} , thus require less energy cost than the case for which \mathbf{j}_v and \mathbf{j}_s are in the same direction. The generation of chiral circulating current implies that there exists a finite kinetic angular momentum in the ground state [41].

The direction of the kinetic angular momentum can be altered by adjusting the intra-component soft-core interactions, which will also change the magnetization of the vortex core. For example, if one exchanges the values of $\tilde{C}_6^{(\uparrow\uparrow)}$ and $\tilde{C}_6^{(\downarrow\downarrow)}$, the places of the two component condensates will be accordingly swapped in the radial separation, thus the magnetization of the vortex core flips into the opposite direction. Notice that the SO coupling fixes the chirality between the spin orientation in the vortex core and the circulating direction of the particle current. As a result, both the canonical and gauge parts of the kinetic angular momentum reverse their directions, and the orientation of the total kinetic angular momentum carried by a crystal cell is altered from z to $-z$ axis [See Figs 2(a)-2(b)].

Phase diagram.—We next map out the phase diagram of the many-body ground states spanned by the Rashba SO coupling and the soft-core interaction strengths. First we devote to the influences of the soft-core interactions by fixing the SO coupling strength at $\kappa = 4 \hbar / M R_c$. It is found that when one of the intra-component soft-core interactions is relatively smaller than the inter-component one with a critical value, the ground state is a spin-polarized superfluid (SPSF) phase, where all particles condense at the component with weaker intra-component

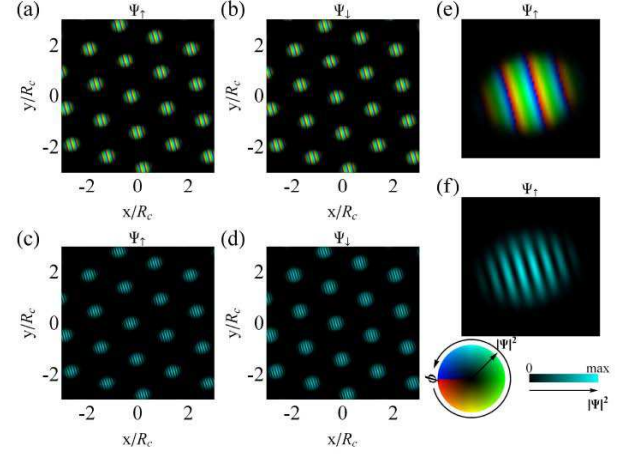


FIG. 4: (Color online) Two typical structures of the non-chiral supersolid. (a)-(b) Plane-wave supersolid. (c)-(d) Standing-wave supersolid. One crystal cell of the plane-wave supersolid and standing-wave supersolid is shown in (e) and (f), respectively. The spin-down-component soft-core interaction strengths are $\tilde{C}_6^{(\downarrow\downarrow)} N = 2200 \hbar^2 R_c^4 / M$ for the PWSS phase and $\tilde{C}_6^{(\downarrow\downarrow)} N = 1875 \hbar^2 R_c^4 / M$ for the SWSS phase. Other parameters are taken as $\tilde{C}_6^{(\uparrow\uparrow)} N = 2500 \hbar^2 R_c^4 / M$, $\tilde{C}_6^{(\uparrow\downarrow)} N = 1250 \hbar^2 R_c^4 / M$, $\kappa = 16 \hbar / M R_c$ and $gN = 1000 \hbar^2 / M$.

soft-core interaction [See Fig. 3(a)]. In this spin-polarized case, the SO coupling becomes irrelevant, and the density and phase are uniformly distributed in space with both the spatial translational symmetry and the time-reversal symmetry conserved.

When the intra-component soft-core interactions $\tilde{C}_6^{(\uparrow\uparrow)}$ and $\tilde{C}_6^{(\downarrow\downarrow)}$ are both stronger than the inter-component soft-core interaction $\tilde{C}_6^{(\uparrow\downarrow)}$, the ground state prefers a non-chiral supersolid phase. In this phase, both of the components have periodic density modulation with the spatial translational symmetry broken, and form a supersolid crystal. Different from the usual supersolid crystal discovered in a system without SO coupling [27–30, 66], the phase distribution in space is nontrivial, and has a linear gradient along some spontaneous direction, implying the breaking of both time-reversal symmetry and spatial rotational symmetry. Each unit cell of the supersolid crystal is very similar to the plane wave phase discovered in a hard-core system with SO coupling [67, 68], as shown in Figs. 4(a), 4(b) and 4(e). From this point of view, we denote this phase as plane-wave supersolid (PWSS) in Fig. 3(a). It should be noted that even though there exists a phase gradient for the PWSS, representing a finite superfluid velocity, the total particle current is zero because the superfluid velocity part \mathbf{j}_v is canceled by the gauge part \mathbf{j}_s . This is very different from the case of CSS, where the superfluid velocity part and gauge part can not cancel each other. Besides, the CSS phase is found to be present in the middle interaction region over a wide parameter range as shown in Fig. 3(a).

The strength of the SO coupling also plays an important role in determining the phase diagram. For strong enough SO coupling strength κ , both the CSS and SPSF phases disappear, and are replaced by another non-chiral supersolid phase as shown in the phase diagram Fig. 3(b). In this new phase, the effect of SO coupling becomes dominant, leading to the presence of spin stripes within each crystal cell [See Figs. 4(c), 4(d) and 4(f)]. Each crystal cell of this supersolid is very similar to the standing wave phase discovered in a hard-core system with SO coupling [67–70], thus we denote this phase as standing-wave supersolid (SWSS). It should be noted that in the SWSS phase there exist two types of translational symmetry breaking, with one related to the formation of supersolid crystal, and the other to the formation of stripes within a crystal cell.

Anomalous phase separation.—In the phase diagram of Fig. 3(b), we find another chiral symmetry broken supersolid phase within the intermediate region of SO coupling strength. This phase is referred as anomalous chiral supersolid (ACSS) phase, and is distinct from the CSS phase in two aspects. Firstly, the spin texture of the radial phase separation is reversed for the ACSS state, such that the spin component with weaker intra-component interaction forms a higher-density shell about the one with stronger interaction [See Fig. 5]. For a two-component BEC without SO coupling, this form of phase separation is in general energetically unfavorable [71], replaced by forming a lower-density shell in the component with stronger interaction. However, such an anomalous structure can be stabilized in the present system with a fairly strong SO coupling. This can be understood by noting that stronger SO coupling requires larger angular momentum, which can be more easily sustained by a higher-density shell.

Secondly, as the chirality between the spin orientation and the circulating particle current is preserved by the specific form of SO coupling, the change in the radial phase separation will induce a change of sign for the angular momentum, which can be read from the canonical part of the angular momentum related to the phase gradient as shown in Fig. 5. That is to say, one can alter the direction of the angular momentum by adjusting the SO coupling strength. This observation goes beyond the intuitive sense that adjusting SO strength can only change the magnitude of the angular momentum.

Rashba vs Dresselhaus effects on the chirality.—The emergence of chiral particle current is attributed to the special form of the Rashba-type SO coupling, which has been previously demonstrated to introduce rigorous mathematical mapping to a chiral magnet with Dzyaloshinskii-Moriya interaction [14]. An interesting question is whether one can change the chirality by changing the type of SO coupling from Rashba to Dresselhaus. In consideration of this, one recalls that the circulating direction of the particle current is related to the

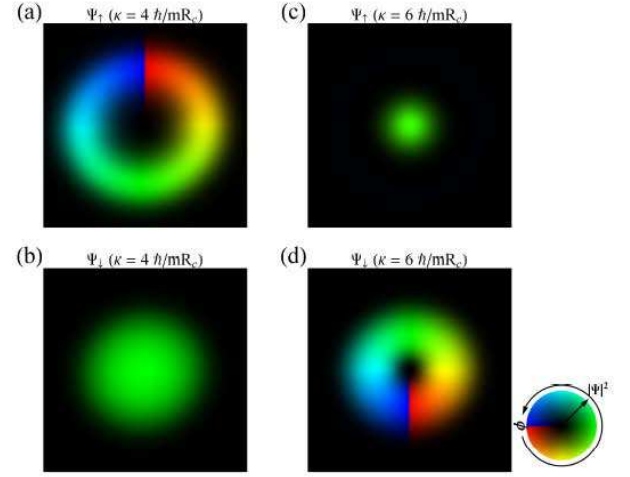


FIG. 5: (Color online) Spin-orbit-coupling effects on the phase separation. (a)-(b) Normal phase separation with weaker SO coupling $\kappa = 4 \hbar/mR_c$. (c)-(d) Anomalous phase separation with stronger SO coupling $\kappa = 6 \hbar/mR_c$. The density and phase distributions of one crystal cell are represented by brightness and color, respectively. The interatomic interactions are fixed at $\tilde{C}_6^{(\uparrow\uparrow)}N = 2500 \hbar^2 R_c^4/M$, $\tilde{C}_6^{(\downarrow\downarrow)}N = 1250 \hbar^2 R_c^4/M$, $\tilde{C}_6^{(\uparrow\downarrow)}N = 1250 \hbar^2 R_c^4/M$ and $gN = 1000 \hbar^2/M$. The size of each square in this image is R_c on a side.

spin matrix vector σ of the SO coupling as $\mathbf{j}_s = \kappa \Psi^\dagger \sigma \Psi$. Changing the form of SO coupling from Rashba-type to Dresselhaus-type will be accompanied by a space reflection of the spin along the y -axis, and lead to a new spin matrix vector $\sigma' = \sigma_x \hat{e}_x - \sigma_y \hat{e}_y$. In such case, the gauge part of the particle current is rewritten as $\mathbf{j}_s = \kappa \Psi^\dagger \sigma' \Psi$, thus may lead to a change of chirality. Numerical simulations demonstrate that the Dresselhaus SO coupling lead to an opposite chirality of the particle current with that of the Rashba case as shown in Fig. 2.

Conclusion.—In summary, we have mapped out the ground-state phase diagram of spin-orbit-coupled soft-core Bose gases. A surprising finding is the existence of an exotic chiral supersolid phase, which shows many unique properties: (i) The chiral symmetry is broken and accompanied by the spontaneous emergence of circulating particle current in each crystal cell. (ii) The system gains a finite angular momentum in a non-rotating frame, whose direction can be altered by adjusting the strengths of spin-orbit coupling or interatomic interaction. (iii) In some parameter regions, the chiral supersolid manifests anomalous behaviour of phase separation. (iv) The Rashba and Dresselhaus spin-orbit coupling lead to opposite chiralities in the supersolid. All of these aspects break through the conventional knowledge of generating angular momentum and phase separation, and bring new perspectives on the physics of spin-orbit coupling and supersolid phenomena.

This work was supported by the NMFSEID under

Grant No. 61127901; the NKRD under Grants No. 2013CB922000; the NSFC under Grants No. 11434011, No. 11522436, No. 11547126 and No. 11547194; the Youth Innovation Promotion Association of Chinese Academy of Sciences under Grant No. 2015334; the Research Funds of Renmin University of China under Grants No. 10XNL016 and No. 16XNLQ03.

* Electronic address: xfzhang@ntsc.ac.cn

† Electronic address: wzhangl@ruc.edu.cn

‡ Electronic address: szhang@ntsc.ac.cn

- [1] B. A. McGuire, P. B. Carroll, R. A. Loomis, I. A. Finneran, P. R. Jewell, A. J. Remijan, and G. A. Blake, Discovery of the interstellar chiral molecule propylene oxide ($\text{CH}_3\text{CHCH}_2\text{O}$), *Science* **352**, 1449 (2016).
- [2] M. Yoon, R. Srirambalaji, and K. Kim, Homochiral metal-organic frameworks for asymmetric heterogeneous catalysis, *Chem. Rev.* **112**, 1196 (2012).
- [3] C. Kallin and J. Berlinsky, Chiral superconductors, *Rep. Prog. Phys.* **79**, 054502 (2016).
- [4] H. Weng, C. Fang, Z. Fang, B. A. Bernevig, and X. Dai, Weyl semimetal phase in noncentrosymmetric transition-metal monophosphides, *Phys. Rev. X* **5**, 011029 (2015).
- [5] K.-S. Ryu, L. Thomas, S.-H. Yang, and S. Parkin, Chiral spin torque at magnetic domain walls, *Nat. Nanotechnol.* **8**, 527 (2013).
- [6] S. Emori, U. Bauer, S.-M. Ahn, E. Martinez, and G. S. D. Beach, Current-driven dynamics of chiral ferromagnetic domain walls, *Nat. Mater.* **12**, 611 (2013).
- [7] G. Chen, T. Ma, A. T. N'Diaye, H. Kwon, C. Won, Y. Wu, and A. K. Schmid, Tailoring the chirality of magnetic domain walls by interface engineering, *Nat. Commun.* **4**, 2671 (2013).
- [8] K. Shibata, X. Z. Yu, T. Hara, D. Morikawa, N. Kanazawa, K. Kimoto, S. Ishiwata, Y. Matsui, and Y. Tokura, Towards control of the size and helicity of skyrmions in helimagnetic alloys by spin-orbit coupling, *Nat. Nanotechnol.* **8**, 723 (2013).
- [9] Y.-J. Lin, K. Jiménez-García, and I. B. Spielman, Spin-orbit-coupled Bose-Einstein condensates, *Nature* **471**, 83 (2011).
- [10] P. Wang, Z.-Q. Yu, Z. Fu, J. Miao, L. Huang, S. Chai, H. Zhai, and J. Zhang, Spin-orbit coupled degenerate Fermi gases, *Phys. Rev. Lett.* **109**, 095301 (2012).
- [11] L. W. Cheuk, A. T. Sommer, Z. Hadzibabic, T. Yefsah, W. S. Bakr, and M. W. Zwierlein, Spin-injection spectroscopy of a spin-orbit coupled Fermi gas, *Phys. Rev. Lett.* **109**, 095302 (2012).
- [12] L. Huang, Z. Meng, P. Wang, P. Peng, S.-L. Zhang, L. Chen, D. Li, Q. Zhou, and J. Zhang, Experimental realization of two-dimensional synthetic spin-orbit coupling in ultracold Fermi gases, *Nat. Phys.* **12**, 540 (2016).
- [13] Z. Wu, L. Zhang, W. Sun, X.-T. Xu, B.-Z. Wang, S.-C. Ji, Y. Deng, S. Chen, X.-J. Liu, and J.-W. Pan, Realization of two-dimensional spin-orbit coupling for Bose-Einstein condensates, *Science* **354**, 83 (2016).
- [14] X.-Q. Xu and J. H. Han, Emergence of chiral magnetism in spinor Bose-Einstein condensates with Rashba coupling, *Phys. Rev. Lett.* **108**, 185301 (2012).
- [15] S.-S. Zhang, W.-M. Liu, and H. Pu, Itinerant chiral ferromagnetism in a trapped Rashba spin-orbit-coupled Fermi gas, *Phys. Rev. A* **93**, 043602 (2016).
- [16] V. Galitski and I. B. Spielman, Spin-orbit coupling in quantum gases, *Nature* **494**, 49 (2013).
- [17] J. Dalibard, F. Gerbier, G. Juzeliūnas, and P. Öhberg, Colloquium: Artificial gauge potentials for neutral atoms, *Rev. Mod. Phys.* **83**, 1523 (2011).
- [18] N. Goldman, G. Juzeliūnas, P. Öhberg, and I. B. Spielman, Light-induced gauge fields for ultracold atoms, *Rep. Prog. Phys.* **77**, 126401 (2014).
- [19] H. Zhai, Spin-orbit coupled quantum gases, *Int. J. Mod. Phys. B* **26**, 1230001 (2012).
- [20] H. Zhai, Degenerate quantum gases with spin-orbit coupling: a review, *Rep. Prog. Phys.* **78**, 026001 (2015).
- [21] W. Yi, W. Zhang, and X. L. Cui, Pairing superfluidity in spin-orbit coupled ultracold Fermi gases, *Sci. China: Phys. Mech. Astron.* **58**, 014201 (2015).
- [22] J. Zhang, H. Hu, X. J. Liu, and H. Pu, Fermi gases with synthetic spin-orbit coupling, *Annu. Rev. Cold At. Mol.* **2**, 81 (2014).
- [23] C. Wu, Unconventional Bose-Einstein condensations beyond the “no-node” theorem, *Mod. Phys. Lett. B* **23**, 1 (2009).
- [24] Y. Deng, J. Cheng, H. Jing, C.-P. Sun, and S. Yi, Spin-orbit-coupled dipolar Bose-Einstein condensates, *Phys. Rev. Lett.* **108**, 125301 (2012).
- [25] R. M. Wilson, B. M. Anderson, and C. W. Clark, Meron ground state of Rashba spin-orbit-coupled dipolar bosons, *Phys. Rev. Lett.* **111**, 185303 (2013).
- [26] S. Gopalakrishnan, I. Martin, and E. A. Demler, Quantum quasicrystals of spin-orbit-coupled dipolar bosons, *Phys. Rev. Lett.* **111**, 185304 (2013).
- [27] N. Henkel, R. Nath, and T. Pohl, Three-dimensional roton excitations and supersolid formation in Rydberg-excited Bose-Einstein condensates, *Phys. Rev. Lett.* **104**, 195302 (2010).
- [28] C.-H. Hsueh, Y.-C. Tsai, K.-S. Wu, M.-S. Chang, and W. C. Wu, Pseudospin orders in the supersolid phases in binary Rydberg-dressed Bose-Einstein condensates, *Phys. Rev. A* **88**, 043646 (2013).
- [29] M. Boninsegni and N. V. Prokof'ev, Colloquium: Supersolids: What and where are they? *Rev. Mod. Phys.* **84**, 759 (2012).
- [30] M. Boninsegni, Supersolid phases of cold atom assemblies, *J. Low. Temp. Phys.* **168**, 137 (2012).
- [31] S. Balibar, The enigma of supersolidity, *Nature* **464**, 176 (2010).
- [32] A. F. Andreev and I. M. Lifshitz, Quantum theory of defects in crystals, *Sov. Phys. JETP* **29**, 1107 (1969).
- [33] G. V. Chester, Speculations on Bose-Einstein condensation and quantum crystals, *Phys. Rev. A* **2**, 256 (1970).
- [34] A. J. Leggett, Can a solid be “superfluid”? *Phys. Rev. Lett.* **25**, 1543 (1970).
- [35] E. Kim and M. H. W. Chan, Probable observation of a supersolid helium phase, *Nature* **427**, 225 (2004).
- [36] D. Bohm, Note on a theorem of Bloch concerning possible causes of superconductivity, *Phys. Rev.* **75**, 502 (1949).
- [37] Y. Ohashi and T. Momoi, On the Bloch theorem concerning spontaneous electric current, *J. Phys. Soc. Jpn.* **65**, 3254 (1996).
- [38] K. W. Madison, F. Chevy, W. Wohlleben, and J. Dalibard, Vortex formation in a stirred Bose-Einstein con-

- densate, *Phys. Rev. Lett.* **84**, 806 (2000).
- [39] J. R. Abo-Shaer, C. Raman, J. M. Vogels, and W. Ketterle, Observation of vortex lattices in Bose-Einstein condensates, *Science* **292**, 476 (2001).
 - [40] Y.-J. Lin, R. L. Compton, K. Jiménez-García, J. V. Porto, and I. B. Spielman, Synthetic magnetic fields for ultracold neutral atoms, *Nature* **462**, 628 (2009).
 - [41] See Supplemental Materials, which includes Refs.[9, 13, 27, 28, 42–52], for more information about the numerical details, experimental relevance, analysis of the angular momentum, and future prospects.
 - [42] W. Bao, I.-L. Chern, and F. Y. Lim, Efficient and spectrally accurate numerical methods for computing ground and first excited states in Bose-Einstein condensates, *J. Comput. Phys.* **219**, 836 (2006).
 - [43] W. Han, G. Juzeliūnas, W. Zhang, and W.-M. Liu, Supersolid with nontrivial topological spin textures in spin-orbit-coupled Bose gases, *Phys. Rev. A* **91**, 013607 (2015).
 - [44] R. Beals and J. Szmigielski, Meijer G-functions: A gentle introduction, *Notices Amer. Math. Soc.* **60**, 866 (2013).
 - [45] Z.-F. Xu, L. You, and M. Ueda, Atomic spin-orbit coupling synthesized with magnetic-field-gradient pulses, *Phys. Rev. A* **87**, 063634 (2013).
 - [46] B. M. Anderson, I. B. Spielman, and G. Juzeliūnas, Magnetically generated spin-orbit coupling for ultracold atoms, *Phys. Rev. Lett.* **111**, 125301 (2013).
 - [47] X. Luo, L. Wu, J. Chen, Q. Guan, K. Gao, Z.-F. Xu, L. You, and R. Wang, Tunable atomic spin-orbit coupling synthesized with a modulating gradient magnetic field, *Sci. Rep.* **6**, 18983 (2016).
 - [48] T. Yefsah, R. Desbuquois, L. Chomaz, K. J. Günter, and J. Dalibard, Exploring the thermodynamics of a two-dimensional Bose gas, *Phys. Rev. Lett.* **107**, 130401 (2011).
 - [49] B. M. Anderson, G. Juzeliūnas, V. M. Galitski, and I. B. Spielman, Synthetic 3D spin-orbit coupling, *Phys. Rev. Lett.* **108**, 235301 (2012).
 - [50] M. DeMarco and H. Pu, Angular spin-orbit coupling in cold atoms, *Phys. Rev. A* **91**, 033630 (2015).
 - [51] K. Sun, C. Qu, and C. Zhang, Spin-orbital-angular-momentum coupling in Bose-Einstein condensates, *Phys. Rev. A* **91**, 063627 (2015).
 - [52] R. Barnett, G. R. Boyd, and V. Galitski, SU(3) spin-orbit coupling in systems of ultracold atoms, *Phys. Rev. Lett.* **109**, 235308 (2012).
 - [53] C.-J. Wu, I. Mondragon-Shem, and X.-F. Zhou, Unconventional Bose-Einstein condensations from spin-orbit coupling, *Chin. Phys. Lett.* **28**, 097102 (2011).
 - [54] S. Sinha, R. Nath, and L. Santos, Trapped two-dimensional condensates with synthetic spin-orbit coupling, *Phys. Rev. Lett.* **107**, 270401 (2011).
 - [55] H. Hu, B. Ramachandhran, H. Pu, and X.-J. Liu, Spin-orbit coupled weakly interacting Bose-Einstein condensates in harmonic traps, *Phys. Rev. Lett.* **108**, 010402 (2012).
 - [56] B. Ramachandhran, B. Opanchuk, X.-J. Liu, H. Pu, P. D. Drummond, and H. Hu, Half-quantum vortex state in a spin-orbit-coupled Bose-Einstein condensate, *Phys. Rev. A* **85**, 023606 (2012).
 - [57] The right-hand (left-hand) rule indicates that the right (left) fingers are curled in the direction of circulation and the right (left) thumb points in the spin orientation in the vortex core.
 - [58] Z. F. Xu, R. Lü, and L. You, Emergent patterns in a spin-orbit-coupled spin-2 Bose-Einstein condensate, *Phys. Rev. A* **83**, 053602 (2011).
 - [59] S.-W. Su, I.-K. Liu, Y.-C. Tsai, W. M. Liu, and S.-C. Gou, Crystallized half-skyrmions and inverted half-skyrmions in the condensation of spin-1 Bose gases with spin-orbit coupling, *Phys. Rev. A* **86**, 023601 (2012).
 - [60] Z. F. Xu, Y. Kawaguchi, L. You, and M. Ueda, Symmetry classification of spin-orbit-coupled spinor Bose-Einstein condensates, *Phys. Rev. A* **86**, 033628 (2012).
 - [61] E. Ruokokoski, J. A. M. Huhtamäki, and M. Möttönen, Stationary states of trapped spin-orbit-coupled Bose-Einstein condensates, *Phys. Rev. A* **86**, 051607(R) (2012).
 - [62] Z.-F. Xu, S. Kobayashi, and M. Ueda, Gauge-spin-space rotation-invariant vortices in spin-orbit-coupled Bose-Einstein condensates, *Phys. Rev. A* **88**, 013621 (2013).
 - [63] S.-W. Su, S.-C. Gou, Q. Sun, L. Wen, W.-M. Liu, A.-C. Ji, J. Ruseckas, and G. Juzeliūnas, Rashba-type spin-orbit coupling in bilayer Bose-Einstein condensates, *Phys. Rev. A* **93**, 053630 (2016).
 - [64] T. Ozawa and G. Baym, Striped states in weakly trapped ultracold Bose gases with Rashba spin-orbit coupling, *Phys. Rev. A* **85**, 063623 (2012).
 - [65] A. L. Fetter, Vortex dynamics in spin-orbit-coupled Bose-Einstein condensates, *Phys. Rev. A* **89**, 023629 (2014).
 - [66] C.-H. Hsueh, T.-C. Lin, T.-L. Horng, and W. C. Wu, Quantum crystals in a trapped Rydberg-dressed Bose-Einstein condensate, *Phys. Rev. A* **86**, 013619 (2012).
 - [67] C. Wang, C. Gao, C.-M. Jian, and H. Zhai, Spin-orbit coupled spinor Bose-Einstein condensates, *Phys. Rev. Lett.* **105**, 160403 (2010).
 - [68] S.-C. Ji, J.-Y. Zhang, L. Zhang, Z.-D. Du, W. Zheng, Y.-J. Deng, H. Zhai, S. Chen, and J.-W. Pan, Experimental determination of the finite-temperature phase diagram of a spin-orbit coupled Bose gas, *Nat. Phys.* **10**, 314 (2014).
 - [69] T.-L. Ho and S. Zhang, Bose-Einstein condensates with spin-orbit interaction, *Phys. Rev. Lett.* **107**, 150403 (2011).
 - [70] Y. Li, L. P. Pitaevskii, and S. Stringari, Quantum tricriticality and phase transitions in spin-orbit coupled Bose-Einstein condensates, *Phys. Rev. Lett.* **108**, 225301 (2012).
 - [71] D. S. Hall, M. R. Matthews, J. R. Ensher, C. E. Wieman, and E. A. Cornell, Dynamics of component separation in a binary mixture of Bose-Einstein condensates, *Phys. Rev. Lett.* **81**, 1539 (1998).

SUPPLEMENTARY MATERIALS

Numerical details. We investigate the many-body effects based on the Gross-Pitaevskii mean-field theory. The many-body ground states can be obtained by numerically minimizing the Hamiltonian functional given by Eq. (1) in the main text. Alternatively, in the numerical simulations one can use the backward-forward Euler Fourier-pseudospectral discretization [42, 43] with the Fourier transformation of $U_{ij}(\mathbf{r})$ represented by the Meijer's G -function as $\tilde{U}_{ij}(\mathbf{k}) = \tilde{C}_6^{(ij)}/R_{ij}^4(\pi/3)G_{06}^{40}\left[\left(\frac{R_{ij}\mathbf{k}}{6}\right)^6\middle|_{0,1/3,2/3,2/3,0,1/3}\right]$ [44].

Experimental relevance. We consider the experimental feasibility. The spin-orbit (SO) coupling may be realized by using periodic pulsed magnetic fields [45–47], and the soft-core interactions can be experimentally induced by Rydberg dressing technique based on off-resonant two-photon excitation [27, 28]. The two-dimensional geometry can be realized by imposing a strong harmonic potential $V(z) = M\omega_z^2 z^2/2$ along the axial direction with the characteristic length $a_{hz} = \sqrt{\hbar/M\omega_z} \ll R_{ij}$. For this case, the contact interaction strengths can be calculated using $g_{ij} = \sqrt{8\pi}(\hbar^2/M)(a_{ij}/a_{hz})$ with a_{ij} the s -wave scattering length [48]. The soft-core interaction strengths and blockade radius induced by Rydberg dressing can be calculated using $\tilde{C}_6^{(ij)} = v_i v_j C_6^{(ij)}$ and $R_{ij} = (C_6^{(ij)}/2\hbar\Delta_{ij})^{1/6}$, where $C_6^{(ij)}$ are the van der Waals (vdW) interaction strengths between two identical or diverse Rydberg atoms, and the parameters $\Delta_{ij} = (\Delta_i + \Delta_j)/2$ and $v_i = (\Omega_i/2\Delta_i)^2$ are related to the detunings Δ_i and Rabi frequencies Ω_i of the lasers used in the Rydberg dressing [28]. For simplicity, here we only focus on the case that the blockade radii R_{ij} are the same, labeled as R_c .

Analysis of the angular momentum. In a SO-coupled system, the gauge-invariant angular momentum, i.e., the “kinetic angular momentum” to be identified in laboratory experiments, is written as $\hat{L}_z^{\text{kin}} = \hat{L}_z + M\kappa\mathbf{r} \times \boldsymbol{\sigma}$ with $\hat{L}_z = \mathbf{r} \times \hat{\mathbf{p}} = -i\hbar\frac{\partial}{\partial\varphi}$ being the canonical part. Thus, the expectation value of the kinetic angular momentum carried by one particle in each crystal cell can be expressed as $l_z^{\text{kin}} = \int (M\mathbf{r} \times (\mathbf{j}_s + \mathbf{j}_v))_z d\mathbf{r} = \int (M\mathbf{r} \times \mathbf{j})_z d\mathbf{r}$, where S_0 limits the range of integration within one crystal cell. As a result, the generation of chiral circulating current \mathbf{j} implies that there exists a finite angular momentum in the ground state of the supersolid phase. According to the numerical results shown in Figs. 1e-1f of the main text, the wave function for each crystal cell can be well approximated by $\Phi(r, \varphi) = [-if(r)e^{-i\varphi}, g(r)]^T$ with $f(r)$ and $g(r)$ being some positive-definite functions relevant to the radial density distributions. Obviously, the expectation value of the canonical angular momentum is a constant and takes the value of $l_z = -\hbar/2$. However, the gauge part of the kinetic angular momentum is proportional to the strength of the SO coupling, and can be expressed as $l_z^s = \int (M\mathbf{r} \times \mathbf{j}_s)_z d\mathbf{r} = 4\pi M\kappa \int_{S_0} f(r)g(r)r^2 dr$.

Future prospects. The SO-coupled soft-core Bose gas investigated here is a multi-parameter complicated system. For simplicity, some of the parameters such as the spin-exchange interaction are ignored, and many other parameters involving the hard-core interaction, the inter-component soft-core interaction and the blockade radius are taken with fixed values. At the same time, the soft-core interactions are supposed to be much stronger than the hard-core ones. A natural expansion of our work is to investigate the ground-state phase diagram within the full parameter space, and discuss the influences of the not yet studied parameters. It should be predicted that the competition between the hard-core and soft-core interactions, as well as the blockade radius, will lead to many other exotic phases in the SO-coupled soft-core system.

In addition to the Rashba and Dresselhaus types, many new forms of SO coupling such as the NIST [9], Weyl [49], USTC [13] types as well as the angular SO coupling [50, 51] and SU(3) SO coupling [52] have been designed in hard-core systems, some of which has no analogue in condensed matter (or any other matter). The introduction of soft-core interactions in these systems will open up a new avenue in cold atom physics, and make important breakthroughs in discovering novel states of matter and quantum phenomena.